Chemical Engineering Journal 158 (2010) 333–344

Contents lists available at ScienceDirect

Chemical Engineering Journal

journal homepage: www.elsevier.com/locate/cej

Easy γ-to-α transformation of zirconium phosphate/polyphenylphosphonate salts: Porosity and hydrogen physisorption

Ernesto Brunet*, Hussein M.H. Alhendawi, Carlos Cerro, María José de la Mata, Olga Juanes, Juan Carlos Rodríguez-Ubis

Department of Organic Chemistry, Faculty of Sciences, Universidad Autónoma de Madrid, 28049 Madrid, Spain

ARTICLE INFO

Article history:
Received 13 October 2009
Received in revised form 14 January 2010
Accepted 19 January 2010

Keywords:
Zirconium phosphate
Organic–inorganic materials
Layered materials
Pillared structures
Hydrogen physisorption

ABSTRACT

The preparation of organic–inorganic materials based on the topotactic exchange reactions of the γ phase of zirconium phosphate and polyphenyl bisphosphonates is reported. The treatment of these materials with hypophosphoric, phosphorous and methylphosphonic acids easily led to an isomerization of the γ phases to their α allotropes. These reactions rendered finely engineered supramolecular structures by means of mild, simple processes performed in the solid–liquid interface. This kind of clean γ-to-α transformations described in our work has few precedents in the literature and allows for the effortless preparation of libraries of similar materials in which the testing of a given set of properties versus subtle structural changes may be easily performed. Using this rationale we have produced materials able to store up to 1.7% (w/w) of H_2 at 77 K and 1 atm with such high ultramicroporosity that the DOE-goal H_2 densities established for 2010 could be complied at pressures well below 5 atm.

1. Introduction

Layered zirconium phosphate (ZrP) may be considered as an excellent chemical-engineering tool, kind of carving board, where organic phosphonates can be orderly deposited leading to materials whose structural features and applications would only be limited by the imagination of the researcher. The two main allotropes of zirconium phosphate are known as α and γ phases [1]. Fig. 1 depicts a reduced model of two consecutive layers. Slate-like macroscopic particles are typically formed by less than a hundred layers (Fig. 2).

The α- and γ-ZrP phases share the same elemental composition but slightly different empirical formulae [$Zr(HPO_4)_2$ for α and $Zr(PO_4)(H_2PO_4)$ for γ]. Their structure is significantly different (Fig. 1). The α-ZrP phase bears a single kind of phosphates, bonded through three oxygen atoms to three different Zr. The reminder P–OH bonds lay almost perpendicular to the average plane of the layer thus sticking out on both sides towards the interlaminar region. In turn, γ-ZrP abides two different types of phosphates, one internal and another external, bonded through four and two oxygen atoms, respectively, to the corresponding number of different metals. The external phosphate, pointing two P–OH groups towards the interlayer region, is relatively labile in that it can be mildly replaced by other phosphorous functions. This exchange reaction is topotactic (it preserves the integrity of the γ-ZrP layered structure), may be multiple and sequentially effected [2] and provides the γ-ZrP phase with a reactive versatility not shown by its α-ZrP counterpart [3]. All these facts praise γ-ZrP as an extremely useful layered scaffold where organic molecules can be easily confined and thus unexpected properties can be effectively wielded (smoothly chemically driven, yet drastic porosity changes, supramolecular chirality, photoinduced charge-transfer processes, molecular recognition and hosting, etc.) [4].

Along these lines, we recently reported on various topotactic phosphate-exchange reactions in succession over γ-ZrP. For instance, the treatment with hypophosphite of γ-ZrP pillared with polyethylenoxadiphosphonates led to a second topotactic exchange of the remaining surface phosphates and to an overall polarity change of the layers which gave rise to drastic porosity changes induced by simple base titration in the liquid–solid interface (Fig. 3) [5]. This process, extremely easily to perform in practice, has complex conceptual implications at the supramolecular level that should lead to new ideas concerning chemical engineering of new materials.

In a more recent preliminary paper we reported on similar hypophosphite reactions with γ-ZrP pillared with rigid *p*-terphenyldiphosphonate, leading to microporous materials with promising abilities for efficient hydrogen physisorption [6]. However, on the contrary to what happened in γ-ZrP pillared with flexible polyethylenoxadiphosphonates, hypophosphite did not lead to a second topotactic exchange but isomerized the whole structure to pillared α-ZrP with *p*-terphenyldiphosphonate, a mixed phosphate/phosphonate α-phase which would have been

* Corresponding author. Tel.: +34 914973926; fax: +34 914973966.
E-mail address: ernesto.brunet@uam.es (E. Brunet).

1385-8947/$ – see front matter © 2010 Elsevier B.V. All rights reserved.
doi:10.1016/j.cej.2010.01.040

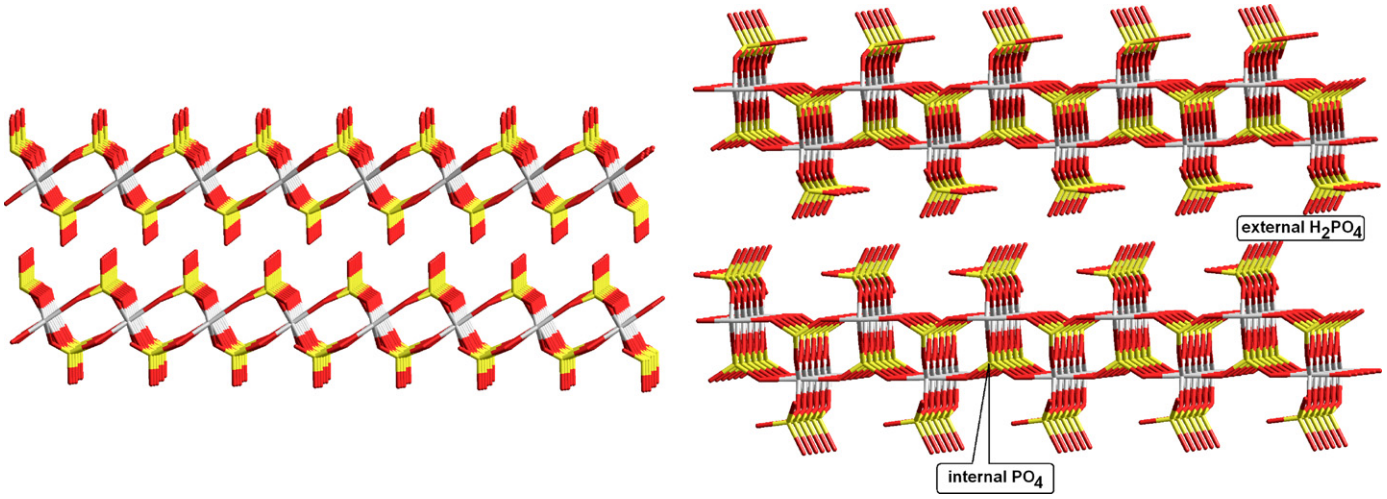

Fig. 1. Molecular models of a portion of two consecutive lamelae of α- (left) and γ-ZrP phases, showing for the α-phase one kind of phosphates (HPO_3: P, yellow; O, red) and a single layer Zr atoms (light gray) and two kinds of phosphates (internal PO_4 and external H_2PO_4) and a bi-layer of Zr atoms for the γ-phase (H atoms are not shown). (For interpretation of the references to color in this figure caption, the reader is referred to the web version of the article.)

very difficult or impossible to be made by direct synthesis [3]. We hereby give a full report of our findings and describe further experiments concerning this isomerization and the creation of porous materials with different polarity characteristics as a workbench to systematically test their hydrogen-storage abilities.

2. Materials and methods

2.1. Materials

4,4′-Diiodobiphenyl, 1,1′:4′,1″-terphenyl and the rest of the necessary reagents were purchased from Aldrich and used as received. γ-ZrP was prepared as previously reported [7].

2.2. Characterizations

Solution ^{1}H and ^{13}C NMR spectra were recorded on Bruker AV-300 spectrometers at 300 and 75 MHz, respectively. Chemical shifts were given in ppm relative to TMS using the corresponding solvent signal as internal reference. Solid-state ^{13}C NMR spectra were recorded under cross-polarization (unless otherwise indicated) and magic-angle techniques (CP-MAS) on a Bruker AV-400 WB spectrometer. Chemical shifts were given in ppm relative to TMS using adamantane as external standard. Powder X-ray diffraction (XRD) patterns were recorded on either Bruker-AXS D8 or PANalytical X'Pert PRO Detector X'celerator diffractometers using Cu Kα radiation (λ = 0.154 nm) at 40 kV, 30 mA, a scanning rate of 5° min^{-1}, and a 2θ angle ranging from 3° to 70°. TGA was performed on a TA instrument TGA Q 500 at a rate of 5° min^{-1}. DTG curves were calculated using the software of the instrument. ICP-MS was carried out on a Perkin-Elmer Sciex Elan 6000 instrument.

2.3. Preparation of diphosphonic acids

(*a*) *4,4″-Diiodo-1,1′:4′,1″-terphenyl* [8]: 1,1′:4′,1″-Terphenyl (4.6 g, 20 mmol), iodine (10.2 g, 40 mmol) and 98% periodic acid (1.83 g, 8 mmol) were added to 75 mL of a 10:2:0.3 (v/v/v) mixture of acetic acid, water and sulfuric acid and the mixture stirred and heated to 100 °C. When the mixture thickened, another portion of the solvent (ca. 35 mL) was added in order to keep the stirring effective for 24 h. After cooling at room temperature, the mixture was filtered. The resulting solid was washed with 500 mL portions of water, 10% sodium thiosulfate and water again. The crude product was recrystallized from toluene yielding 7.6 g (80%) of a white solid. Solid-state ^{13}C RMN (CP-MAS) δ (ppm): 98.0 (I–*C*); 126.0 (I–Ph–*C*CH), 134.8 (I–CCH), 136.0 (I–CCCH), 139.4 (I–CCCC and I–Ph–*C*); elemental analysis (%), calcd. for $C_{18}H_{12}I_2$: C, 44.84; H, 2.51; found: C, 44.77; H, 2.53. MS (EI) *m*/*z*: 481.9 $[M]^+$.

(*b*) The corresponding diiodopolyphenyl derivative (7.4 mmol) and anhydrous nickel chloride (175 mg, 1.4 mmol) were placed in a dried flask under Ar. Triethylphosphite (7.0 mL, 40.8 mmol) was added to the mixture and the reaction was heated to 140 °C

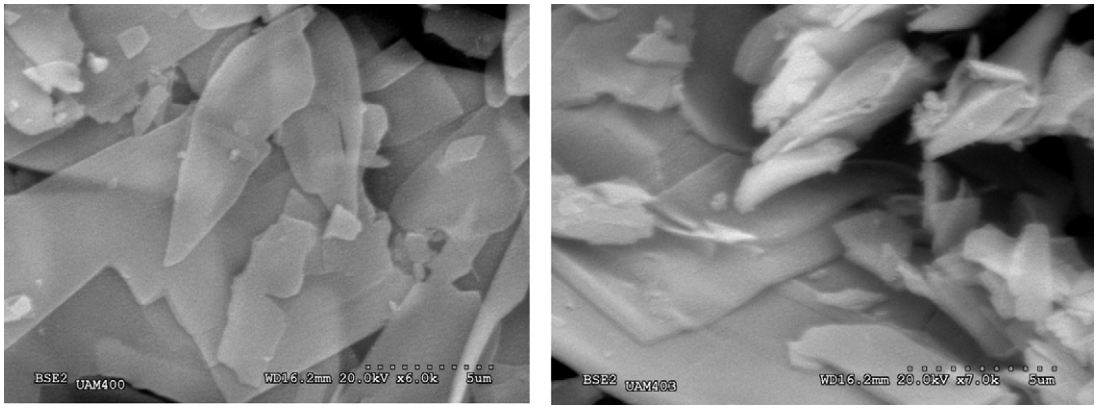

Fig. 2. SEM images of materials **γB40** (left) and **γT40** (see text and Table 1).

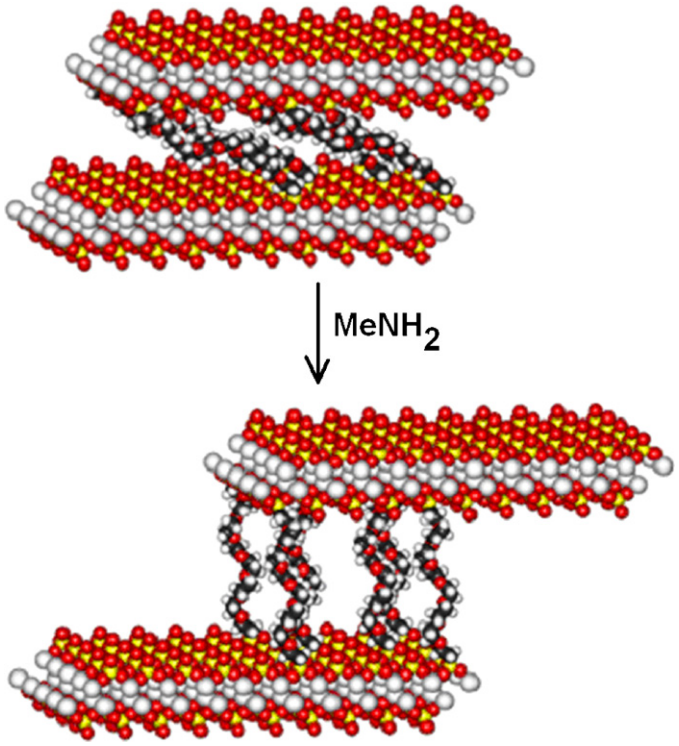

Fig. 3. Schematic representation of the drastic porosity changes induced by simple base titration suffered by γ-ZrP pillared with polyethylenoxadiphosphonates in the liquid–solid interface (see text).

for 16 h. The mixture was then cooled and the excess of triethylphosphite distilled under vacuum. The remainder residue was dissolved in CH_2Cl_2, filtered over celite and the solvent removed at reduced pressure. The resulting solid was recrystallized from CH_2Cl_2/Hexane yielding 80–90% of the pure product as a white powder.

2.4. Tetraethyl biphenyl-4,4′-diylbis(phosphonate)

^{1}H NMR ($CDCl_3$) δ (ppm): 1.36 (t, $^3J_{HH}$ = 7.1 Hz, 12H, $POCH_2CH_3$); 4.15 (m, 8H, $POCH_2CH_3$); 7.37 (m, 4H, PC*H*); 7.81 (m, 4H, PCCHC*H*); ^{13}C NMR ($CDCl_3$) δ (ppm): 16.0 (d, $^3J_{CP}$ = 8.0 Hz, $POCH_2CH_3$); 61.8 (d, $^2J_{CP}$ = 6.0 Hz, $POCH_2CH_3$); 126.9 (PCCH); 126.5 (d, $^1J_{CP}$ = 180.0 Hz, P*C*); 132.1 (PCCH*C*H); 143.5 (PCCHCH*C*); elemental analysis (%), calcd. for $C_{20}H_{28}P_2O_6$: C, 56.34; H, 6.62; found: C: 56.39; H, 6.59; MS (FAB+)*m*/*z*: 427.2 $[M+1]^+$.

2.5. Tetraethyl 1,1′:4′,1″-terphenyl-4,4″-diylbis(phosphonate)

^{1}H NMR ($CDCl_3$) δ (ppm): 1.37 (t, $^3J_{HH}$ = 7.05 Hz, 12H, $POCH_2CH_3$); 4.16 (m, 8H, $POCH_2CH_3$); 7.72 (s, 4H); 7.74 (m, 4H, PCC*H*); 7.93 (m, 4H, PCCHC*H*); ^{13}C NMR ($CDCl_3$) δ (ppm): 16.4 (d, $^3J_{CP}$ = 6.50 Hz, $POCH_2CH_3$); 62.2 (d, $^2J_{CP}$ = 5.40 Hz, $POCH_2CH_3$); 127.1 (d, $^2J_{CP}$ = 15.3 Hz, P–CCH); 127.3 (d, $^1J_{CP}$ = 189.6 Hz, P–*C*); 128.6 (P–Ph–CCCH); 132.4 (d, $^3J_{CP}$ = 10.3 Hz, P–CCCH); 139.8 (P–Ph–*C*); 144.4 (d, $^4J_{CP}$ = 3 Hz, P–CCCC); elemental analysis (%), calcd. for $C_{26}H_{32}P_2O_6$: C, 62.15; H, 6.42; found: C, 62.08; H, 6.44; MS (FAB+)*m*/*z*: 503.5 $[M+1]^+$.

(c) The corresponding tetraethyl bisphosphonate (2.4 mmol) was dissolved in 10 mL of dry CH_2Cl_2 under Ar and the solution was cooled at 0 °C. Trimethylsilyl iodide (4 mL, 28.2 mmol) was added dropwise and the mixture kept at 0 °C for 8 h. The solvent was then removed *in vacuo* and water (40 mL) was added to the residue with vigorous stirring for 30 min. The mixture was concentrated at reduced pressure and the resulting solid was stirred with several portions of toluene until the color was washed out (99%).

2.6. Biphenyl-4,4′-diylbis(phosphonic acid)

^{1}H NMR [$(CD_3)_2SO$] δ (ppm): 7.97 (m, 8H); ^{13}C NMR [$(CD_3)_2SO$] δ (ppm): 131.5 (d, $^3J_{CP}$ = 9.9 Hz, PCCHCH); 136.1 (d, $^2J_{CP}$ = 15.9 Hz, PCCHCH); 138.1 (d, $^1J_{CP}$ = 180.0 Hz, PC); 146.6 (d, $^4J_{CP}$ = 3.0 Hz, PCCHCHC); elemental analysis (%), calcd. for $C_{12}H_{12}P_2O_6$.: C, 45.88; H, 3.85; found: C, 45.86; H, 3.83; MS (ESI) *m*/*z*: 315.0 $[M+1]^+$.

2.7. 1,1′:4′,1″-Terphenyl-4,4″-diylbis(phosphonic acid)

Solid-state ^{13}C NMR (CP-MAS) δ (ppm): 123.6, 124.8, 126.3, 130.2, 132.1, 136.1, 136.9, 139.2; elemental analysis (%), calcd. for $C_{18}H_{16}P_2O_6$: C, 55.39; H, 4.13; found: C, 55.36; H, 4.09; MS (ESI) *m*/*z*: 391.1 $[M+1]^+$.

2.8. General procedure for the topotactic exchange of aromatic phosphonates into γ-ZrP

A certain amount of γ-ZrP was suspended in a 1:4 mixture of water/acetone heated at 85 °C (350 mL per g of γ-ZrP) and vigorously stirred for 20 min. The phosphonic acid, suspended in a 1:4 mixture of water/acetone (350 mL per g of γ-ZrP), was then slowly added at a constant rate of 0.65 mL/min and the heating at 85 °C continued for three days. The mixture was cooled down and the solid was washed with two portions of water and two portions of acetone (20 mL per g of γ-ZrP). The obtained material was dried at 80 °C for 24 h and stored at 90% relative humidity ($BaCl_2$) for at least three days.

2.9. General procedure for the treatment of γ-ZrP derivatives with hipophosphorous, phosphorous or methylphosphonic acid

The γ-ZrP material exchanged with the diphosphonic acid was suspended in a 0.1 M solution of methylammonium chloride (100 mL per g of material). A 0.1 M solution of methylamine was then slowly added until pH = 7. The solid was washed with two portions of water (20 mL per g of added material) and dried in an oven at 80 °C for 4 h. The commercial hypophosphorous, phosphorous or methylphosphonic acids (50% in water; 15 mL of acid per g of γ-ZrP derivative) was dissolved in a 1:4 mixture of water/acetone (100 mL per g of γ-ZrP derivative). To this solution, which was bubbled with Ar for 10 min, the exchanged γ-ZrP, pre-treated with $MeNH_2$ (see above), and a small amount of the very same diphosphonic acid contained by γ-ZrP were added. The mixture was heated at 85 °C overnight, cooled and washed with two portions of water and two portions of acetone (20 mL per g of added γ-ZrP). The obtained material was dried at 80 °C for 24 h and stored at 90% relative humidity ($BaCl_2$) for at least three days.

2.10. General procedure to neutralize ZrP materials with LiOH

A certain amount of α- or γ-ZrP was suspended in enough 0.1 M LiOH solution (100 mL per g of material) to reach pH = 9 (automatic titroprocessor). The resulting material was washed with three portions of water (20 mL per g of added material), dried at 80 °C for 24 h and stored at 90% relative humidity ($BaCl_2$) for at least three days.

2.11. Measurement of porosity and hydrogen physisorption

Nitrogen and hydrogen physisorption and desorption data were collected on a Micromeritics ASAP 2020 with 50–70 mg of the materials. BET isotherms were measured and analyzed using the

Table 1
Polyphenyldiphosphonate-to-(γ-ZrP) molar ratios used in the topotactic exchange reactions with derivatives **1** and **2** of Scheme 1 and characterization data of the resulting materials.

Material	Ratio	Acid conc.[a] ($M \times 10^{-3}$)	$Zr(PO_4)(H_2PO_4)_{[1-(2x+y)]}([C_6H_4]_nP_2O_6H_2)_x([C_6H_4]_nP_2O_6H_3)_y(H_2O)_z$[b]					DRX (nm)	Integral MAS-^{31}P NMR δ (ppm)[c]			Elemental analysis			
			x	y	z	TGA (%) 150–1000 °C			−16	5	18	Found		Calculated	
						Exp.	Calc.					C%	H%	C%	H%
γB30	0.20	(**1**) 1.0	0.18	0.00	2.0	9.0	9.8	1.65	70	30	0	7.6	2.5	7.6	2.1
γB40	0.44	(**1**) 2.0	0.17	0.05	2.0	10.4	13.4	1.73	60	40	5	9.0	2.2	9.1	2.2
γB55	0.65	(**1**) 2.9	0.16	0.20	1.5	10.9	21.2	1.96	50	50	20	14.0	2.3	13.9	2.1
γB60	1.00	(**1**) 5.0	0.13	0.30	1.5	15.5	26.1	2.11	45	55	30	16.2	2.4	15.9	2.2
γT25	0.20	(**2**) 1.0	0.13	0.00	1.5	9.2	12.8	2.06	75	25	0	8.2	1.8	8.3	1.9
γT35	0.44	(**2**) 2.0	0.16	0.05	2.0	12.6	14.4	1.96	65	35	5	12.5	2.7	12.4	2.3
γT40	0.65	(**2**) 2.9	0.09	0.22	2.0	12.1	24.9	2.20	60	40	25	16.4	2.5	16.7	2.5
γT60	1.00	(**2**) 5.0	0.08	0.35	1.0	16.1	32.0	2.65	50	50	30	22.6	2.7	22.2	2.3

[a] Compounds **1** and **2** as in Scheme 1.
[b] For materials **γB** and **γT**, $n = 2$ or 3 respectively.
[c] The reference integral (100) was taken from the signal at −27 ppm which is omitted in the table (see Fig. 1).

standard software provided by Micromeritics. Highly purified hydrogen (99.9995%) was used to collect the H_2 isotherms at 77 K. Previous to all measurements, the materials were activated *in vacuo* at 120 °C for 16 h to remove any trace of volatile impurities. We found that He was physisorbed in our materials leading to severe errors in the estimation of the dead volumes needed for the calculations. Therefore the volumes of the empty flasks, measured using the He protocol of the ASAP2020, were taken for that purpose. The volume of the small amount of the materials was three to four orders of magnitude lower than that of the flask thus contributing to negligible errors in the measurements of H_2 physisorption. The H_2 isotherms displayed complete reversibility in all samples across the whole range of pressures.

3. Results and discussion

3.1. Preparation and characterization of the materials

The exchange reaction of native γ-ZrP with different amounts of polyphenyl diphosphonic acids (Table 1) in the usual exfoliation conditions (1:4 water–acetone at 80 °C) led to materials named as **γB** (from 4,4′-*b*iphenyl diphosphonic acid; **1** in Scheme 1) and **γT** (from 4,4″-*p*-terphenyl diphosphonic acid; **2** in Scheme 1) whose solid-state "non-CP" MAS (10 kHz) ^{31}P NMR (relaxation delay 20 s) are gathered in Fig. 4.

The spectra of Fig. 4 deserve a word before getting into the details of Table 1. The signals at −27 and −14 ppm correspond to

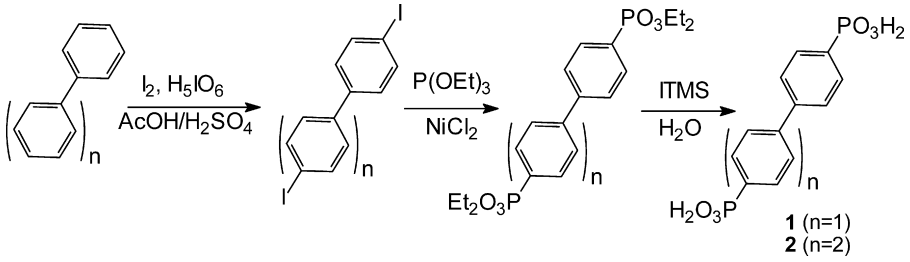

Scheme 1. .

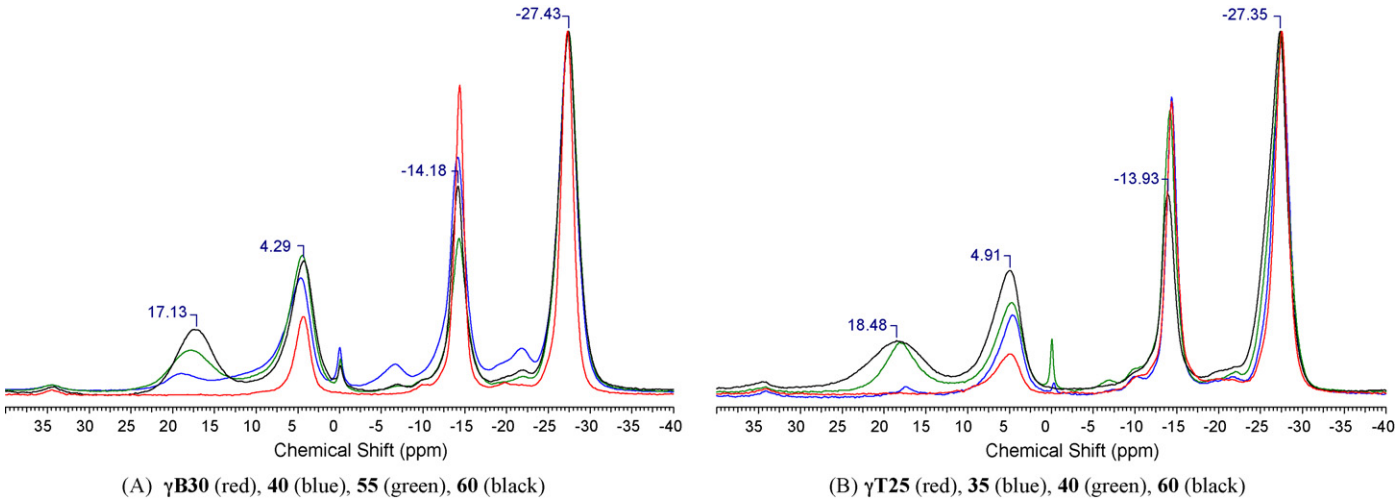

(A) **γB30** (red), **40** (blue), **55** (green), **60** (black) (B) **γT25** (red), **35** (blue), **40** (green), **60** (black)

Fig. 4. Solid-state "non-CP" MAS (10 kHz) ^{31}P NMR (relaxation delay 20 s) of the indicated materials (see text).

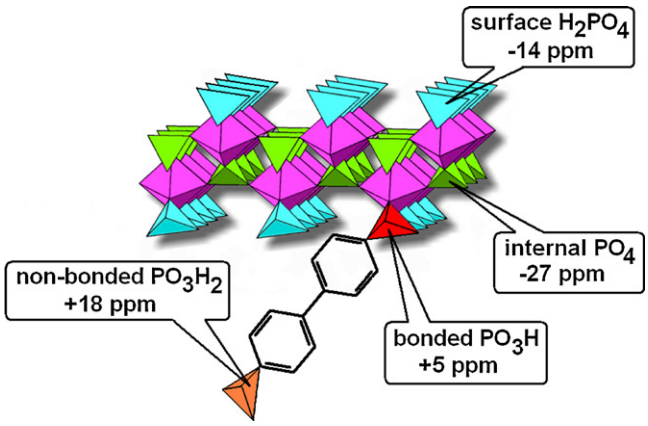

Fig. 5. Schematic depiction of tetrahedral phosphates and phosphonates of exchanged γ-ZrP indicating the observed chemical shifts in the solid-state ^{31}P NMR spectra.

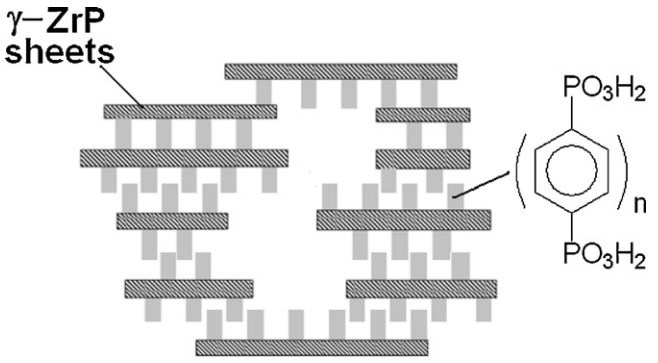

Fig. 6. Schematic representation of a partially pillared structure where some of the diphosphonate groups have failed to cross-link consecutive layers of the inorganic salt.

the internal and surface phosphates of γ-ZrP, respectively (Fig. 5). The phosphonates covalently incorporated to the inorganic layer showed their resonances at ca. 5 ppm. These are the only three signals observed when the exchange reaction was performed with the lowest polyphenyldiphosphonate-to-(γ-ZrP) molar ratio (red spectra in Fig. 4). At higher ratios, a new signal at ca. 18 ppm was observed.

In all cases, the intensity decrease suffered by the signal of the surface phosphates (−14 ppm), relative to the internal ones (−27 ppm), was accounted for by the covalently bonded phosphonates (5 ppm), as an obvious consequence of the topotactic exchange reaction. The new signals at 18 ppm should thus be assigned to non-bonded phosphonates in view of the following. There is ca. 13 ppm difference between the chemical shifts of internal and surface phosphates of γ-ZrP which are different by the number of oxygen atoms bonded to Zr (internal 4, surface 2; difference 2). The more bonds the phosphate sustains with Zr, the more shielded the chemical shift. Therefore, if the signals at 5 ppm belong to the bonded phosphonates which use two oxygen atoms to bind Zr, it looks reasonable that the resonances at 18 ppm ($\Delta\delta$ = 13 ppm) be attributed to phosphonates "using no oxygen atoms" (difference 2) to bind Zr. Therefore, the integral of the signal at 18 ppm directly indicates the number of diphosphonates bonded to γ-ZrP by only one of their ends (*y* in Table 1 and see Fig. 5).

Yet, the main implication of the occurrence of non-bonded phosphonates is that the pillaring should have taken place with many defects forming a structure similar to that schematically depicted in Fig. 6 [3]. We shall comment on this again shortly.

Combining the NMR data with the elemental analysis we obtained the molecular formulae listed in Table 1. It should be noted that γ-ZrP could not take up all diphosphonate available in the reaction medium. For instance, at the polyphenyldiphosphonate-to-(γ-ZrP) molar ratio of 1.0, only half of the put-up organic molecules was incorporated ($x+y$ = 0.43 in Table 1). This should be the result of the limited area surrounding each phosphate (0.36 nm^2) which is smaller than the cross-section of the phenyl groups (0.44 nm^2). This makes that, at the most, only every other phosphate on the layer surface can be replaced by a phosphonate.

The interlayer distance (Table 1) deduced from the powder XRD patterns (Fig. 7) increased regularly with the total amount of incorporated phosphonate. This parameter varied from 1.65 to 2.11 nm and from 1.96 to 2.65 nm for the **γB** and **γT** series, respectively. In order to understand these variations we have performed molecular modeling using the reported crystal structure of γ-ZrP and AM1-refined biphenyl- and *p*-terphenyl diphosphonates. The shortest basal separations were easily reproduced by bonding the organic chains to the opposed faces of two consecutive layers, at the natural angle (ca. 14° with respect to the perpendicular axis) required by the tetrahedral arrangement of the surface phosphates, as shown in Fig. 8A. The larger interlayer distances had to be reproduced by detaching one of the phosphonate groups (Fig. 8B), in agreement with the solid-state ^{31}P NMR spectra (*vide supra*).

The intermediate interlayer distances should arise from disordered structures as that of Fig. 6. This disorder should be also

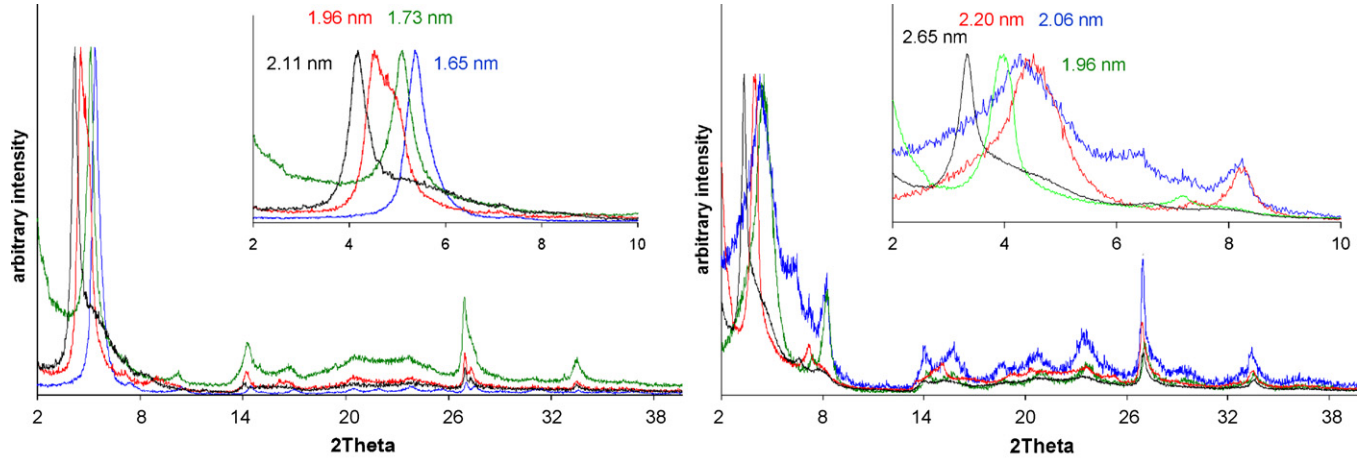

A. γB30 (blue), **40** (green), **55** (red) and **60** (black)

B. γT25 (green), **35** (blue), **40** (red) and **60** (black)

Fig. 7. Powder XRD patterns of the indicated materials.

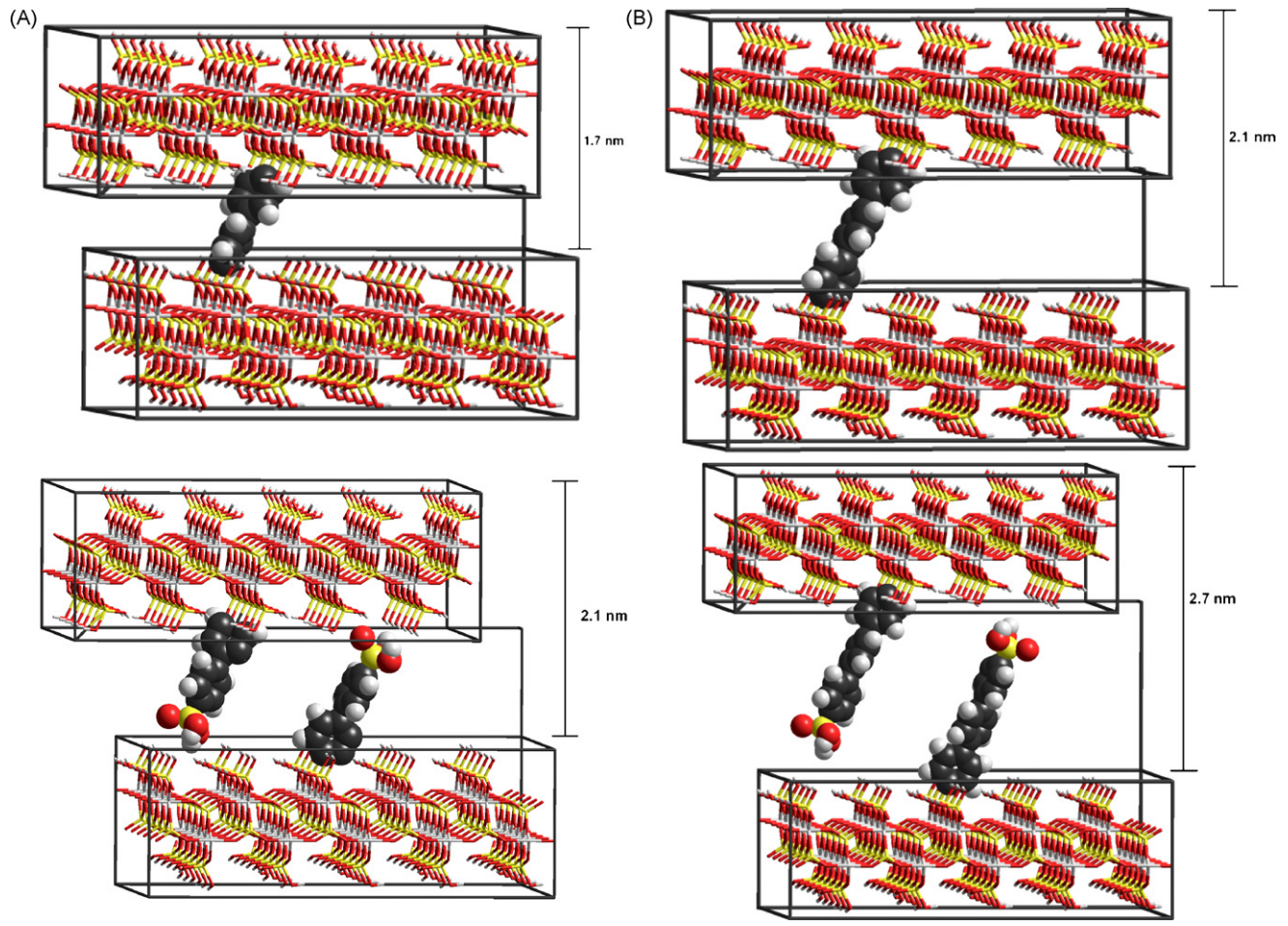

Fig. 8. Simplified molecular models of two consecutive layers of γ-ZrP with the covalently bonded diphosphonates **1** (A) and **2** (B) showing the calculated interlayer distances in agreement with the experimental ones (see text).

responsible of the relatively broad diffractions observed (see for example red traces in the insets of Fig. 7).

The treatment of materials **γB60** and **γT60** with hypophosphite led to new materials named **αB60** and **αT60** after phase α-ZrP, because their "non-CP" MAS (10 kHz) ^{31}P NMR spectra (Fig. 9) resulted very different to those of their precursors and similar to α-ZrP phases.

For instance, the chemical shift of the most intense shielded signal (−21 ppm) is in-between those of the internal (−27 ppm) or surface (−14 ppm) phosphates of γ-ZrP. Since in the latter phase the two types of phosphates are bonded to four and two metals, respectively, the intermediate chemical shift of −21 ppm suggests a phosphate bonded to three metals, *i.e.* belonging to α-ZrP type (Fig. 10). The most deshielded signal (−5.6 ppm) should be assigned

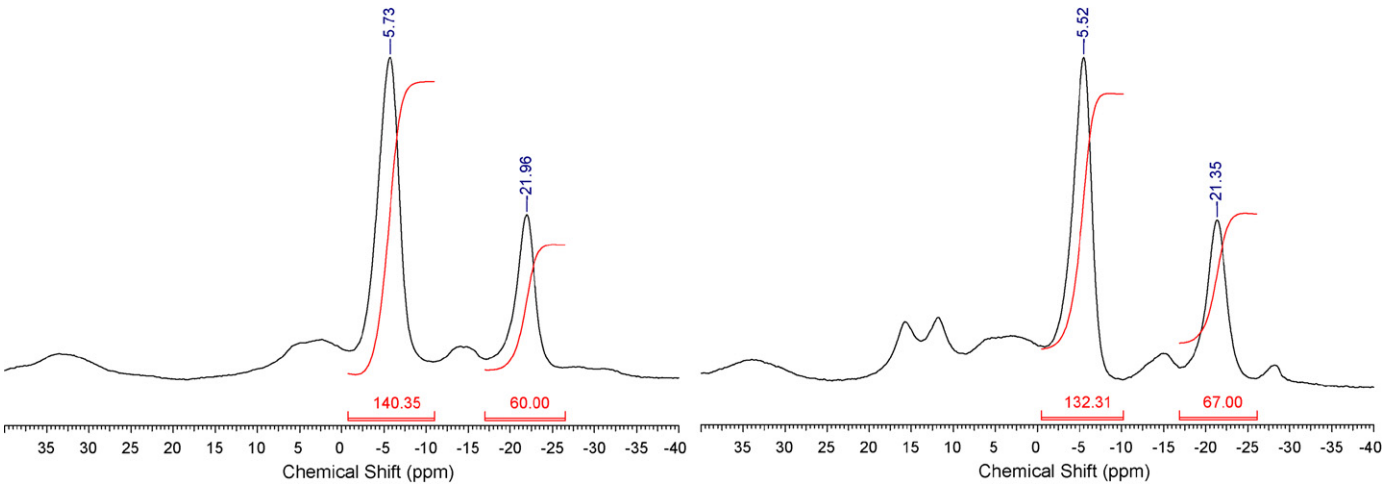

Fig. 9. Solid-state "non-CP" MAS (10 kHz) ^{31}P NMR (relaxation delay 20 s) of materials **αB60** and α**T60** (see text).

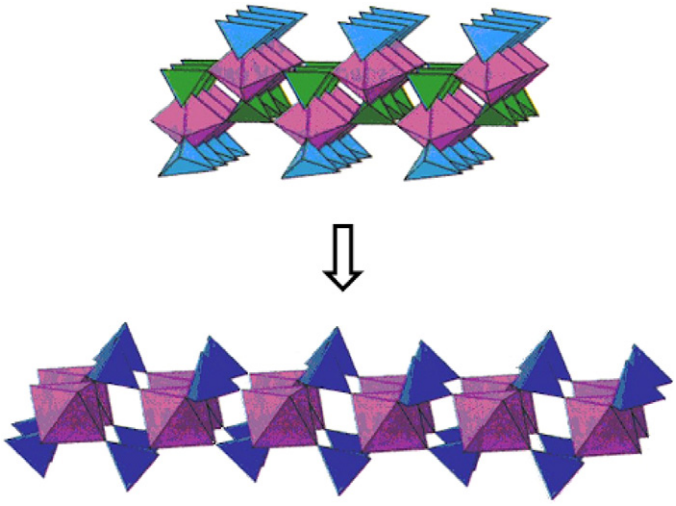

Fig. 10. Isomerization of γ-ZrP to its allotrope α-ZrP.

to the phosphonate groups. The relative integrals of the signals at −5.7 ppm (140–132) and −21 ppm (60–67) suggest that materials **αB60** and **αT60** may be a laminar, pillared α-ZrP with an approximate molecular formula of $[Zr(HOPO_3)_{0.6}(O_3PRPO_3)_{0.7}$; R = $C_{12}H_8$ or $C_{18}H_{12}]$. The phosphonate content of phases **αB60** and **αT60** was thus similar to that of their parents **γB60** and **γT60**. Therefore, the intercourse of hypophosphorous acid induced a reasonably clean isomerization from γ- to α-ZrP without any appreciable loss of polyphenyl diphosphonate. Interestingly, there are no signals to be assigned to free phosphonate groups suggesting that the isomerization rendered a much more uniform phase where broken structures as that of Fig. 3 were less probable. Despite this, crystallinity did not improve much since the powder X-ray diffraction patterns of materials **αB60** and **αT60** displayed relatively broad peaks at 1.36 and 1.88 nm, respectively, distances that are in agreement with the calculated interlayer separation (1.4 and 1.9 nm) for the α-type phase with nearly perpendicular diphenyl and terphenyl columns (Fig. 11).

It should be remarked at this point of the discussion that, in previous work related to pillared γ-ZrP with flexible polyethyleneoxa chains, we observed that hypophosphite smoothly incorporated into the inorganic lamellae by topotactic exchange, *i.e.* without any concomitant isomerization. Hypophosphite has two oxygen atoms that can replace the phosphates on the γ-ZrP surface which are precisely bonded to the metals by two oxygen atoms (sky-blue tetrahedrons in Figs. 5 and 10). The driving force of the γ- to α-ZrP change in the case of **γB60** and **γT60** may be due to a combined effect of the rigidity, polarity and bulkiness of the polyphenyl chains. Another key factor should be the fact that **γB60** and **γT60** are barely pillared, if at all (*vide supra*). Rigidity and polarity should be more important than bulkiness because, despite the large area of the phenyl cross-section, biphenyl- or *p*-terphenyl diphosphonates were able to react with native γ-ZrP respecting its integrity. Yet, once the phases **γB60** and **γT60** were in contact with an hydrolytic medium, the rigid, low polar and high hydrophobic aromatic rings which are inclined ca. 14° in the starting γ-ZrP, have a chance to ameliorate their proximity to the polar inorganic surface. Hence, the barely non-pillared γ-ZrP is completely disrupted and the new α-ZrP with perpendicular columns is formed. Presumably, some of the internal phosphates of γ-ZrP lose one bond with the metal and become α-ZrP type. The whole structure then starts to horizontally stretch up, moving from the typical γ-ZrP pattern with two sheets of Zr metal atoms per layer to the singly leafed α-ZrP layers (Fig. 10). Hypophosphite cannot finally incorporate into the α-ZrP phase because its two oxygen atoms are not enough to compensate for the Zr hexacoordination which is in turn easily fulfilled by the three oxygen atoms coming either from phosphonates or phosphates (navy-blue tetrahedrons in Fig. 10).

We tried the γ-to-α isomerization of material **αT60** with phosphorous and methylphosphonic acids too, with the aim of building materials whose ideally hexagonal pores (*vide infra*) had caps of lower polarity, namely hydrogen or methyl groups, respectively. These reactions rendered materials **αT60H** and **αT60Me** whose solid-state "non-CP" MAS ^{31}P NMR are depicted in Fig. 8. The absence of the γ-phase-signal couple at −27 and −14 ppm indicates that the γ-to-α isomerization did take place again. The signals at ca. −5 ppm should be attributed as usual to the phosphonate groups. The remaining signals in the spectrum of **αT60H** can be assigned to phosphite (−15.6 ppm) and α-type phosphate (−20.4 ppm) in a ratio coincident with the approximate formula $Zr(HPO_3)_{0.4}(HOPO_3)_{0.2}(O_3PC_{18}H_{12}PO_3)_{0.7}$. All efforts to obtain a purer phase were ineffective in our hands.

In the case of **αT60Me**, the signal at 5.1 ppm should be assigned to the methylphosponate and its integral, relative to the phosphonate signal at −5.3 ppm, hints to the formula $Zr(MePO_3)_{0.9}(O_3PC_{18}H_{12}PO_3)_{0.55}$ for **αT60Me**. The appearance of signals at −27.4 and 16.4 ppm suggest the presence of a separate

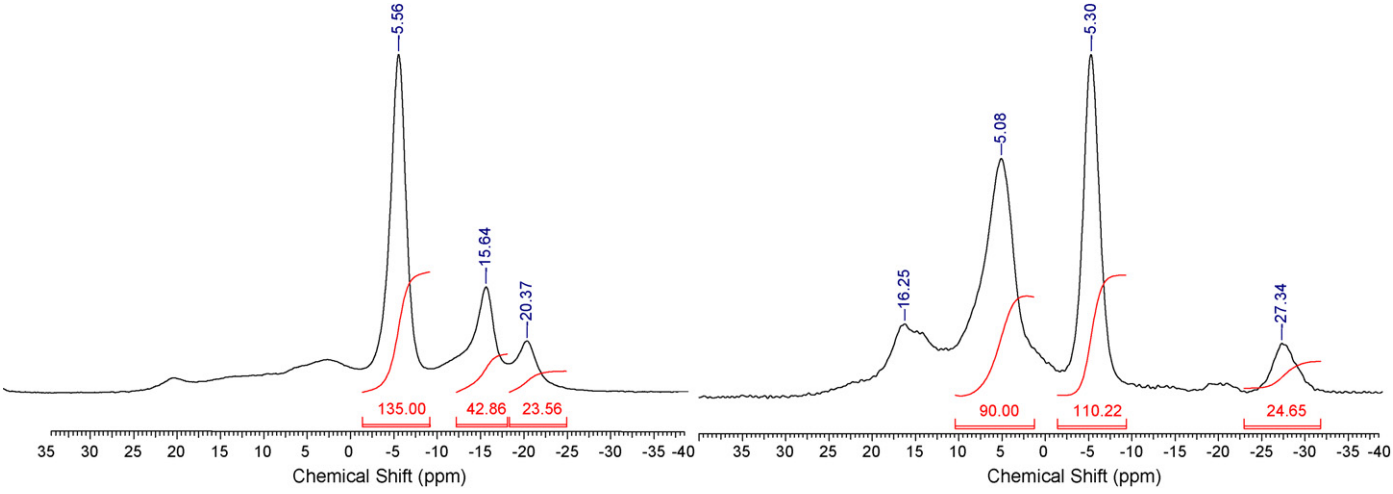

Fig. 11. Solid-state "non-CP" MAS (10 kHz) ^{31}P NMR (relaxation delay 20 s) of materials **αT60H** and **αT60Me** (see text).

Table 2
Relevant characterization data for the materials α-ZrP studied in this work.

Material	α-Zr(RPO$_3$)$_{0.6}$[(C$_6$H$_4$)$_n$P$_2$O$_6$]$_{0.7}$·yH$_2$O			d (nm)	Elemental analysis		BET area m^2/g (% internal)
	RPO$_3$	n	y		%C obs. (calcd.)	%H obs. (calcd.)	
αB60	OH	2	3.2	1.36	23.7 (23.8)	2.9 (3.0)	568 (94%)
αT60	OH	3	2.5	1.88	32.6 (32.6)	3.0 (3.0)	423 (74%)
αB60Li	OLi	2	–	1.38			226 (90%)
αT60Li	OLi	3	–	1.85			229 (69%)
αT60H	H, OH[a]	3	2.5	1.93	33.1 (33.1)	2.7 (3.1)	372 (63%)
αT60Me	CH$_3$[b]	3	0.2	1.87	34.9 (34.6)	2.9 (2.4)	411 (79%)

[a] Zr(HPO$_3$)$_{0.4}$(HOPO$_3$)$_{0.2}$(O$_3$PC$_{18}$H$_{12}$PO$_3$)$_{0.7}$ (see text).
[b] Mixed with Zr(PO$_4$)(Me(OH)PO$_2$) in 15% molar ratio.

methylphosphonate γ-ZrP phase [Zr(PO$_4$)(Me(OH)PO$_2$)] in ca. 15% molar ratio mixed with **αT60Me**. All attempts to avoid this mixture have been unsuccessful.

Finally, neutralization of the acid OH groups of the surface of materials **αB60** and **αT60** with LiOH rendered new composites **αB60Li** and **αT60Li** where the Li$^+$ ions will rest at both ends of the pores, hopefully facilitating hydrogen absorption as it has been suggested in the literature [9].

Therefore, we have handy a battery of similar porous structures with very subtle changes in the floor and ceiling of each layer, namely the presence of OH, OLi, H and Me groups, to asses their influence on porosity and hydrogen physisorption. To the best of our knowledge, no other materials allow for this kind of fine-tuned engineering.

Table 2 summarizes all relevant characterization data for materials α-ZrP that were tried for hydrogen storage as it will be detailed below. It may be seen in the table that the elemental analyses are in excellent accordance with the molecular formulae suggested from ^{31}P NMR. The prepared α-ZrP materials thus resulted uniform regarding their content in the organic moiety.

Fig. 12 shows different viewpoints of idealized models of the α-ZrP phase of formula [Zr(HOPO$_3$)$_{0.6}$(O$_3$PRPO$_3$)$_{0.7}$]$_{100}$ (R = C$_{18}$H$_{12}$). Yet, considering the opposing surfaces of two α-ZrP sheets having 100 + 100 phosphorous places, 70 diphosphonates can be arranged in very different ways as for instance those depicted in Fig. 13. The relatively low resolution of the X-ray diffraction patterns (Fig. 14) suggests that the actual arrangement of diphosphonates should be somewhat disordered.

3.2. Porosity and hydrogen adsorption

Table 3 summarizes all relevant data concerning porosity and hydrogen physisorption of all studied materials. Brunauer–Emmett–Teller method (BET) analysis [10] rendered

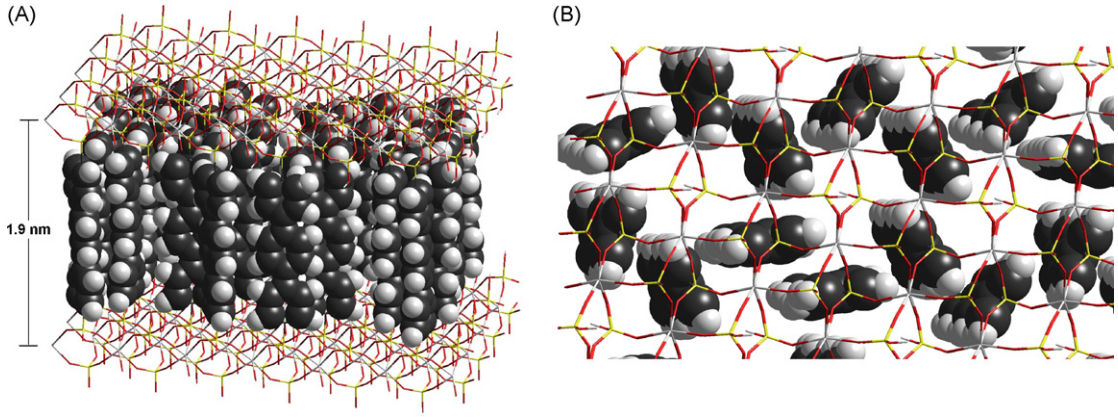

Fig. 12. Idealized models for **αT60** indicating the interlayer calculated distance (the models were identical for **αB60** but with two-phenyl-group columns and a reduced interlayer distance of 1.4 nm).

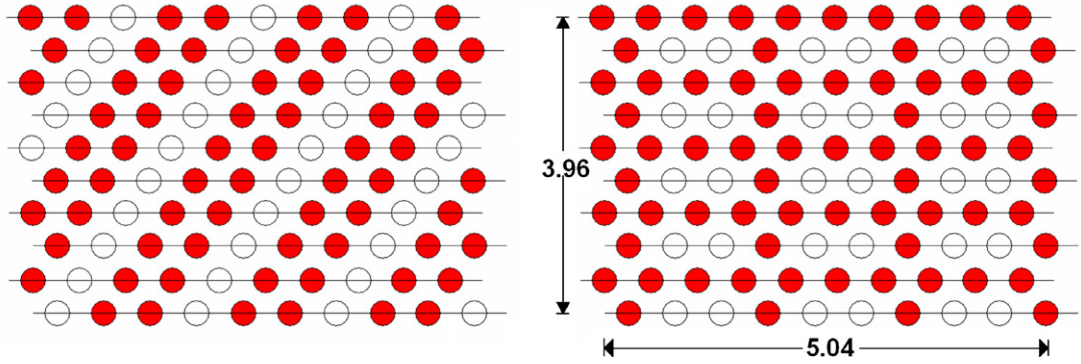

Fig. 13. Two possible ways of arranging 70 diphosphonates (red) within opposing surfaces of two sheets of 100 + 100 phosphorous places in α-ZrP and its measurements in nm. (For interpretation of the references to color in this figure caption, the reader is referred to the web version of the article.)

Table 3
Physisorption data for the indicated materials (see text).

Material (MW g/mol)	d[a]	BET area[b] (%int.)	Volume		800 Torr		15 Torr			500–800 Torr	Saturation	
			Total[c] (D)	Access[d] (%)	%H_2 (g/L)[e]	H_2/MF_{60}[f] (H_2/nm^3)	Slope[g]	H_2/MF_{60}[f]	ΔH_{phys}[h]	Slope[g]	P_{sat}[i] (H_2/MF_{60})[j]	H_2 (g/L)
γB30 (300)	1.65	82 (97)	16.56 (1.80)	8.26 (49.9)	1.4 (24.3)	122 (14.7)	6.0	8	5.3	1.4	1.6 (177)	35.5
γB40 (312)	1.73	54 (69)	17.36 (1.79)	8.59 (49.5)	0.8 (14.5)	76 (8.8)	5.3	8	5.2	0.8	2.9 (184)	35.2
γB40Li (322)	1.70	85 (68)	17.06 (1.88)	8.29 (48.6)	0.9 (16.2)	83 (10.06)	4.7	7	5.0	0.9	2.4 (178)	34.6
γB60 (370)	2.11	124 (89)	21.17 (1.74)	11.46 (54.1)	0.4 (7.7)	49 (4.3)	1.3	2	3.8	0.5	5.5 (245)	38.5
γT25 (307)	2.06	130 (96)	20.67 (1.48)	12.06 (58.4)	1.2 (17.8)	111 (9.2)	4.7	6	5.0	1.4	2.5 (258)	41.5
γT40 (396)	2.20	74 (87)	22.08 (1.79)	12.43 (56.3)	0.7 (13.1)	87 (7.0)	2.0	4	4.0	0.9	3.3 (266)	40.0
γT40Li (377)	2.39	174 (61)	23.98 (1.57)	14.34 (59.8)	0.8 (12.3)	89 (6.19)	6.7	11	5.7	0.7	4.4 (307)	42.5
γT60 (409)	2.65	86 (87)	26.59 (1.53)	15.56 (58.5)	0.6 (9.2)	74 (4.7)	2.0	4	4.0	0.7	4.9 (333)	41.6
αB60 (366)	1.36	568 (94)	21.00 (1.73)	11.32 (53.9)	1.5 (25.4)	161 (14.2)	6.0	10	5.3	2.0	1.6 (242)	38.3
αB60Li (369)	1.38	227 (90)	21.31 (1.73)	11.63 (54.6)	1.6 (27.2)	175 (15.0)	3.3	6	4.7	2.0	1.5 (249)	38.8
αT60 (415)	1.88	423 (74)	29.03 (1.42)	18.16 (62.5)	1.5 (21.8)	190 (10.5)	4.7	8	5.1	1.8	2.2 (389)	44.5
αT60Li (419)	1.85	229 (69)	28.57 (1.46)	17.70 (61.9)	1.7 (24.5)	211 (11.9)	3.3	6	4.7	2.1	1.8 (379)	44.0
αT60H (399)	1.93	384 (63)	29.81 (1.33)	18.93 (63.5)	0.8 (11.2)	100 (5.3)	2.0	4	4.0	1.0	4.3 (405)	45.1
αT60Me (404)	1.87	411 (79)	28.88 (1.39)	18.00 (62.3)	1.4 (19.9)	173 (9.6)	3.3	6	4.3	1.8	2.3 (385)	44.3

[a] Interlayer distance (Table 1).
[b] Specific total area ($m^2\ g^{-1}$) as calculated from the Brunauer–Emmett–Teller method; percentage of internal microporous area between parenthesis.
[c] Total volume in (nm^3) considering two parallelepipeds (Fig. 5) each containing one layer of γ-ZrP of formula $[Zr(PO_4)(H_2PO_4)]_{60}$ (MF_{60}) separated by the experimental interlayer distance; D, estimated density ($g\,cm^{-3}$).
[d] Accessible volume estimated by subtraction the calculated volume of all atoms (QSAR, Hyperchem) from the total volume.
[e] Weight % of physisorbed H_2 and density of stored hydrogen in g/L between parenthesis.
[f] Amount of physisorbed H_2 molecules per MF_{60} and, between parenthesis, density of stored hydrogen in molecules of H_2 per nm^3 of accessible volume.
[g] Slope of the H_2 isotherm at low and high coverage [wt.% $H_2 \times 10^{-3}$ $Torr^{-1}$].
[h] Estimated enthalpy of interaction at low coverage ($kJ\,mol^{-1}$).
[i] Saturation pressure (atm) estimated from the slope at high coverage (500–800 Torr) considering 71.0 g/L or 21.4 H_2/nm^3 (liquid H_2) as the limiting physisorption of H_2.
[j] Estimated amount of physisorbed H_2 molecules per FM_{60} at saturation.

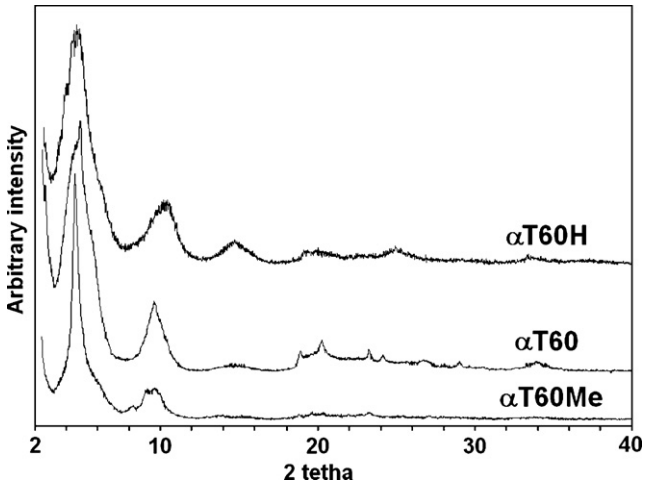

Fig. 14. Powder XRD patterns of the indicated materials.

reasonable specific surfaces, from ca. 130 $m^2\ g^{-1}$ for **γ** materials to a maximum of 568 $m^2\ g^{-}$ for **α** counterparts.

Fig. 15 shows the N_2 isotherm for material **αB60** as a representative example. The shape of the curve, almost identical for all the studied materials, showed little hysteresis and belongs to Ib type [11] with low participation of external area.

By means of Tarazona's model [12], we have obtained the pore size distribution on a selection of the studied materials. Results are graphically gathered in Fig. 16.

Truly pillared materials **γB30** and **γT25** (Fig. 5) with the lowest loading of organic phosphonates in the series, showed the presence of a noticeable distribution of ultramicropores (<0.7 nm; blue traces in Fig. 16A) which were not present in the corresponding materials with larger amount of phosphonates. This is in agreement with the formation of big, irregular pores as those schematically depicted in Fig. 6 when the amount of phosphonates is increased and the structure ceases being pillared, as already discussed from DRX and NMR data (*vide supra*). On the contrary, the diagrams of materials **αB60** and **αT60** which bear a high loading of phosphonates but fully pillared, showed a large distribution of ultramicropores (mauve and red traces in Fig. 16B), in accordance with the molecular modeling of Fig. 9. The incorporation of phosphite or methylphosphonate (as in **αT60H** and **αT60Me**, respectively; blue and green traces in Fig. 16B) appears to lower the participation of ultramicropores.

The H_2 physisorption parameters are listed in Table 3 too. The table also contains some different calculated volumetric features of the materials. For instance, we have calculated the total and accessible volumes contained by two consecutive layers of α- and γ-ZrP of formulae $[Zr(HPO_4)_{2(1-x)}(O_3P(C_6H_4)_nPO_3)_x]_{60}$ and $[Zr(PO_4)(H_2PO_4)_{1-2x}(O_3P(C_6H_4)_nPO_3)_x]_{60}$, respectively, from now on denoted as MF_{60}. We have enclosed the inorganic layers in parallelepipeds, in the way shown in Fig. 8. Therefore, the total volume in Table 3 is that of one parallelepiped enclosing one layer plus that of the interlaminar region, calculated from the experimental interlayer distance as measured by DRX. The accessible space has been estimated by subtracting the volume of all the involved atoms, calculated using the QSAR routine (Gavezotti's atomic radii and grid methods [13]) of HyperChem program [14]. It may be seen that the estimated accessible volume accounts for more than half of the total volume, the **α** series being slightly less dense despite their higher occurrence of organic columns [15]. We have found these volumetric considerations quite useful when assessing H_2 physisorption parameters at 77 K.

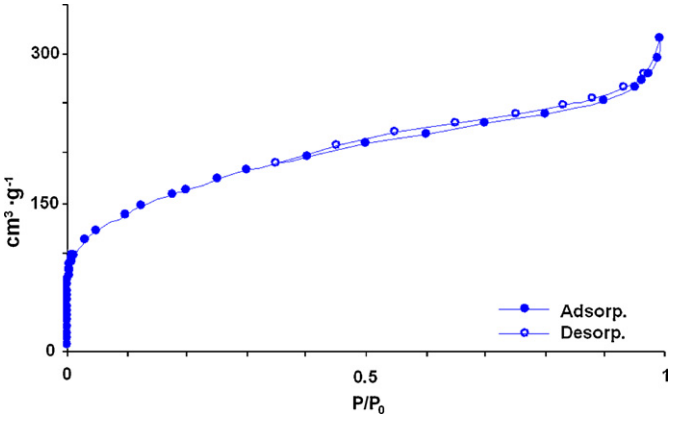

Fig. 15. Pore size distribution of the indicated materials as calculated by Tarazona's model.

In materials **γB** and **γT**, hydrogen physisorption (*cf.* 800 Torr column in Table 3) decreased heavily with the amount of incorporated phosphonates, from interesting values up to ca. 1.3% (w/w) for **γB30** and **γT25** to meagre ca. 0.5% (w/w) for **γB60** and **γT60**. It is remarkable that considering the volumetric calculations made, material **γB30**, the most capable in the **γ** series concerning H_2 physisorption, is able to house 122 hydrogen molecules per MF_{60} (see above) or, in other words, 14.7 hydrogen molecules per nm^3, slightly more than two thirds the density of liquid H_2 (71.0 g L^{-1} or 21.4 hydrogen molecules per nm^3). The presence of Li^+ ions in the **γ** series makes very little effect if any at all.

Hydrogen physisorption was visibly higher in the **α** series, reaching up to 1.7% (w/w) in **αT60Li**, in our belief quite important a result for several reasons. We must stress at this point that the sole consideration of the gravimetric capacity for H_2 physisorption of a given material is rather misleading. It may be seen that comparing with **γB30**, which was able to store 1.4% (w/w), the estimated number of molecules per MF_{60} is almost doubled in **αT60Li** (211 as compared to 122). Yet, since **αT60Li** is less dense and bears more accessible volume than **γB30**, the density of stored H_2 resulted much lower in **αT60Li** (11.9 hydrogen molecules per nm^3), what strongly suggests that this material still have supplementary room to allocate additional H_2 molecules, provided the pressure is somewhat raised. At this moment of the discussion, it would be useful to have a look into the H_2 isotherms (Fig. 17).

No trace of hysteresis was ever observed which means that H_2 is readily desorbed from the materials. The shape of the curves is quite striking because most of them are still very steep at 1 atm (Fig. 17A) suggesting that the materials are far from their saturation point. Unfortunately we lack at this moment of the necessary equipment to measure H_2 physisorption at higher pressures but the following estimations are determining us to perform these measurements at the possible earliest. Let us assume that saturation point is achieved when the physisorbed hydrogen reaches the density of the liquid. Extrapolation of the curves from the slope at their end (column "500–800 Torr" in Table 3) allows the guessing of the necessary pressure to get to that point (column "saturation" in Table 3). In the cases of **γB30** and **αT60Li** the pressures would be rather low (1.6 and 1.8 atm, respectively). However, since the latter is less dense, the hypothetical point of saturation for **αT60Li** would be attained by storing double number of H_2 molecules (377) than **γB30** (177), which would be equivalent to a storage capability of 44 g L^{-1} (total volume considered) for **αT60Li** at an estimated pressure of only 1.8 atm. If the experiments confirm our estimations, this is a storage capacity within the DOE goals for 2010 [16].

The nature of the groups at the floor and ceiling of the pores in the **α** series has an important impact over H_2 storage. From **αT60Me** to **αT60** and to **αT60Li**, capacity varies from 1.4 to 1.7%

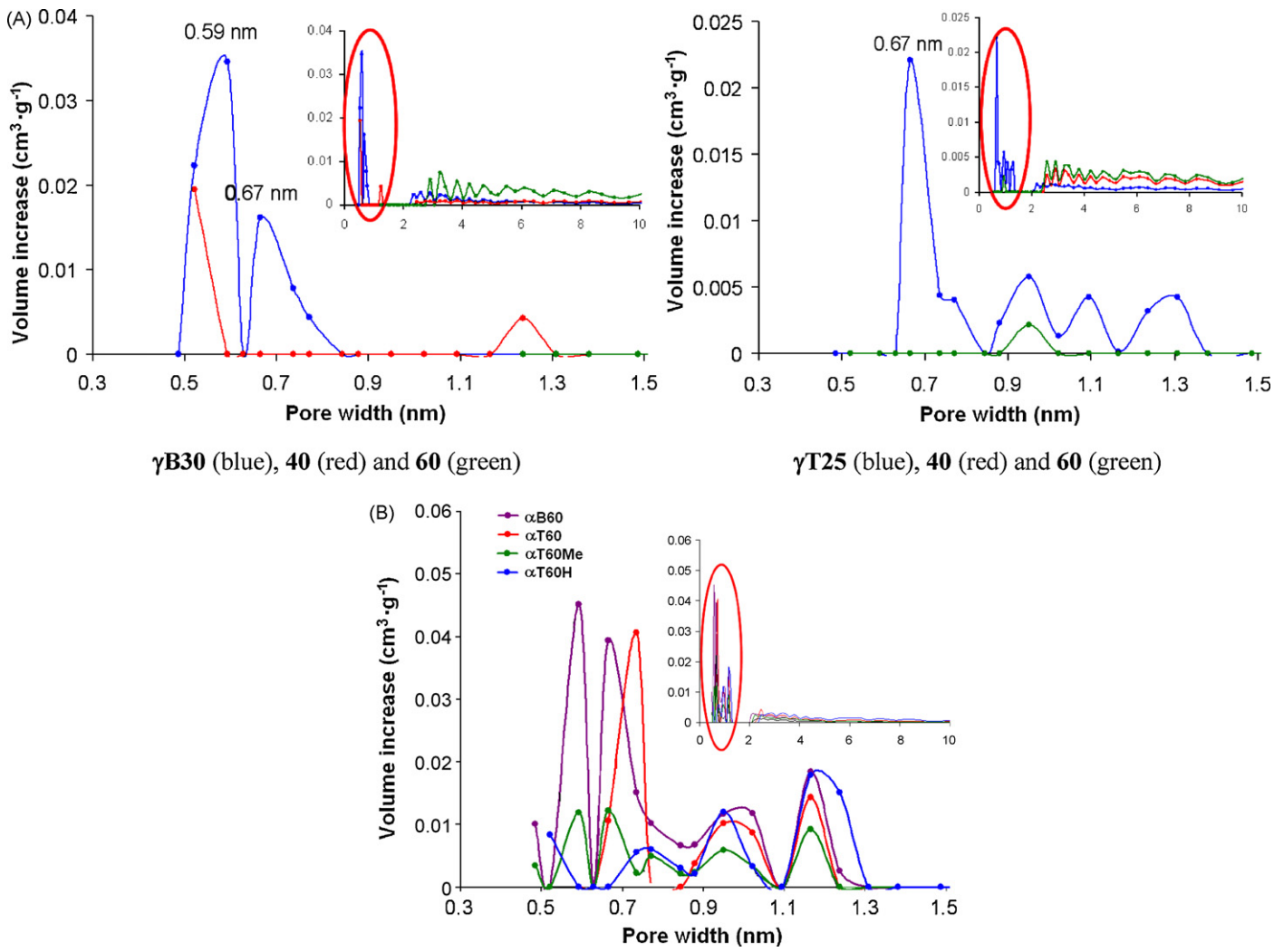

Fig. 16. N_2 isotherm for material **αB60**.

(w/w), clearly showing that polarity is quite important a factor to facilitate H_2 physisorption. The fact that **αT60H**, the less polar in the series, is able to store only 0.8% (w/w) confirms that assumption. Nevertheless, the inspection of the physisorption isotherms at their beginning is puzzling (*cf.* Fig. 14B and column "15 Torr" in Table 3). The slope at this point of the physisorption is assumed to be directly proportional to the affinity for the surface of the empty material of the very first H_2 molecules reaching the pores. Using the literature data [17] one can estimate the energy of interaction at very low H_2 coverage (ΔH_{phys} in Table 3). It may be seen that **αT60Li** is far from bearing the highest ΔH_{phys} but, all things considered, **αT60Li** is the material of all tested in this work having the largest storage capacity for H_2. On the contrary, material **γT40Li** with the largest ΔH_{phys} value ends up storing only 0.8% (w/w) of H_2. It appears that the first 11 molecules that enter the model MF_{60} matrix of **γT40Li** in the first 15 Torr (Table 3), do it with the highest

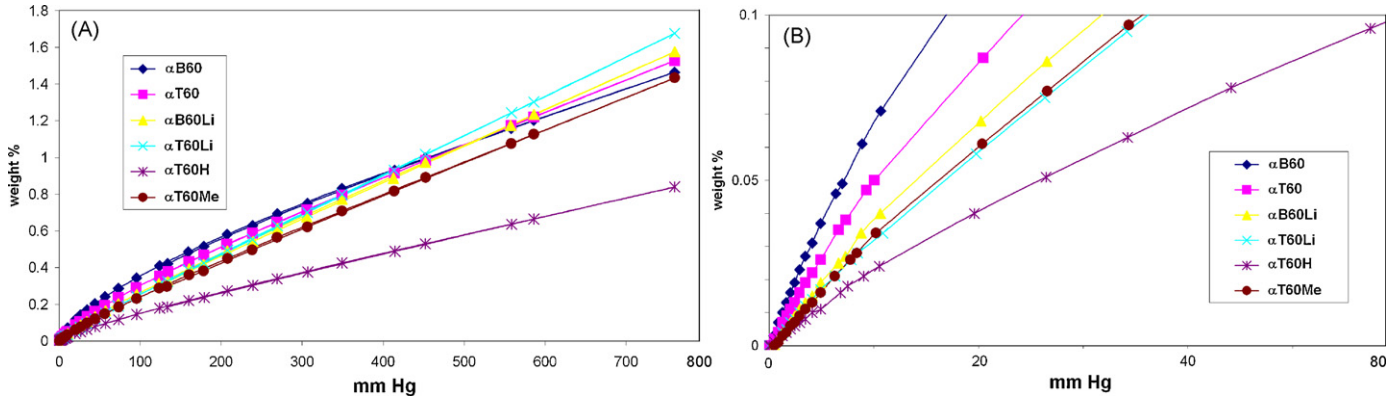

Fig. 17. H_2 isotherms at 77 K of the α series.

affinity in the series. Unfortunately, the relatively higher density of the γ-ZrP series, precludes this material from storing sensible amounts of H_2.

4. Conclusion

Layered ZrP continues showing its versatility. Its synthesis and transformation involve hydrothermal procedures easy to carry out with extremely simple equipment which makes quite affordable the possible scaling-up of the processes. In this paper we have incorporated simple, easy-to-make organic molecules with the result of the building of different organic–inorganic scaffolds tried for their porosity properties and their ability to store hydrogen. We have shown that with relatively little effort, the supramolecular structures may be finely engineered by means of reactions performed in the solid–liquid interface in mild conditions. For instance, the γ-ZrP structure containing polyphenyl diphosphonates have been cleanly isomerized to α-ZrP by reaction with hypophosphite, phosphite or methylphosphonate, the latter two being incorporated to the layered structures. While α-ZrP structures may be achieved by direct synthesis, the kind of γ-to-α transformation described in our work has no precedent in the literature and allows for the effortless preparation of libraries of similar materials in which the checking of a given set of properties against subtle structural changes may be easily performed. This is a unique feature of layered ZrP which we plan to keep on exploiting in different areas. Using this rationale we have produced materials able to store up to 1.7% (w/w) of H_2 at 77 K and 1 atm with such high ultra microporosity that the DOE-goal H_2 densities for 2010 are expected to be complied at pressures as low as 2 atm. Further work concerning this aspect is under progress.

Acknowledgements

This work has been performed under the indirect support of ERCROS-Farmacia S.A. to which we are deeply grateful. Unfortunately, we do regret that the financial backing from the Ministry of Science and Education of Spain has just drastically decreased after the generous grants received in the near past (MAT2002-03243, MAT2006-00570).

References

[1] A. Clearfield, W.L. Duax, A.S. Medina, G.D. Smith, J.R. Thomas, Mechanism of ion exchange in crystalline zirconium phosphates. I. Sodium ion exchange of γ-zirconium phosphate, Phys. Chem. 73 (1969) 3424;
G. Alberti, U. Costantino, Recent progress in the intercalation chemistry of layered γ-zirconium phosphate and its derivatives and future perspectives for their use in catalysis, J. Mol. Catal. 27 (1984) 235;
A. Clearfield, J.M. Kalnins, On the mechanism of ion exchange in zirconium phosphates. XXIII. Exchange of first row divalent transition elements on γ-zirconium phosphate, J. Inorg. Nucl. Chem. 40 (1978) 1933;
N.J. Clayden, Solid-state nuclear magnetic resonance spectroscopic study of γ-zirconium phosphate, J. Chem. Soc., Dalton Trans. (1987) 1877.

[2] E. Brunet, M.J. de la Mata, O. Juanes, J.C. Rodriguez-Ubis, Sensitized luminescence of lanthanides within the walls of polyethylenoxa-pillared γ-zirconium phosphate, Chem. Mater. 16 (2004) 1517;
E. Brunet, M. Alonso, C. Cerro, O. Juanes, J.C. Rodríguez-Ubis, A.E. Kaifer, A luminescence and electrochemical study of photoinduced electron transfer within the layers of zirconium phosphate, Adv. Funct. Mater. 17 (2007) 1603.

[3] A. Clearfield, Z. Wang, P. Bellinghausen, Highly porous zirconium aryldiphosphonates and their conversion to strong bronsted acids, J. Solid State Chem. 167 (2002) 376.

[4] G. Alberti, E. Brunet, C. Dionigi, O. Juanes, M.J. de la Mata, J.C. Rodriguez-Ubis, R. Vivani, Shaping solid-state supramolecular cavities: chemically induced accordion-like movement of γ-zirconium phosphate containing polyethylenoxide pillars, Angew. Chem. Int. Ed. 38 (1999) 3351;
E. Brunet, M.J. de la Mata, O. Juanes, H.M.H. Alhendawi, C. Cerro, J.C. Rodríguez-Ubis, Solid-state reshaping of nanostructured cristal: supremolecular of layered materials derived from polyethylenoxa-pillared zirconium phosphate, Tetr. Asym. 17 (2006) 347;
E. Brunet, M. Alonso, M.J. de la Mata, S. Fernandez, O. Juanes, O. Chavanes, J.C. Rodriguez-Ubis, Covalent bonding of phosphonates of fullerene and Ru complexes to γ-zirconium phosphate as a template for building chemical devices in the solid state, Chem. Mater. 15 (2003) 1232.

[5] E. Brunet, M.J. de la Mata, O. Juanes, J.C. Rodriguez-Ubis, Solid-state reshaping of crystals: flash increase in porosity of zirconium phosphate-hypophosphite that contains polyethylenoxa diphosphonate pillars, Angew. Chem. Int. Ed. 43 (2004) 619.

[6] E. Brunet, H.M.H. Alhendawi, C. Cerro, M.J. de la Mata, O. Juanes, J.C. Rodriguez-Ubis, Hydrogen storage in a highly porous solid derived from γ-zirconium phosphate, Angew. Chem. Int. Ed. 45 (2006) 6918.

[7] E. Brunet, M. Huelva, R. Vazquez, O. Juanes, J.C. Rodriguez-Ubis, Covalent bonding of crown ethers to γ-zirconium phosphate—new layered ion exchangers showing selective recognition, Chem. Eur. J. 2 (1996) 1578.

[8] M.R. Unroe, B.A. Reinhardt, One pot synthesis of p-polyphenyls via the intramolecular cyclization of 3-(dimethylamino)hex-5-en-1-ynes, Synthesis 11 (1987) 981.

[9] Q. Sun, P. Jena, Q. Wang, M. Marquez, First-principles study of hydrogen storage on $Li_{12}C_{60}$, J. Am. Chem. Soc. 128 (2006) 9741.

[10] S. Brunauer, P.H. Emmett, E. Teller, Adsorption of gases in multimolecular layers, J. Am. Chem. Soc. 60 (1938) 309.

[11] F. Rouquerol, J. Rouquerol, K. Sing, Adsorption by Powders and Porous Solids—Principles, Methodology and Applications, Academic Press, London, 1999.

[12] R. Evans, U.M.B. Marconi, P. Tarazona, Fluids in narrow pores: adsorption, capillary condensation, and critical points, J. Chem. Phys. 84 (1986) 2376.

[13] A. Gavezzotti, The calculation of molecular volumes and the use of volume analysis in the investigation of structured media and of solid-state organic reactivity, J. Am. Chem. Soc. 105 (1983) 5220.

[14] N. Bodor, Z. Gabanyi, C.K. Wong, A new method for the estimation of partition coefficient, J. Am. Chem. Soc. 111 (1989) 3783.

[15] Density values in Table 3 have been estimated from the total volume and the molecular weight of the corresponding MF_{60}.

[16] http://www.sc.doe.gov/bes/hydrogen.pdf.

[17] (a) J.Y. Lee, L. Pan, S.P. Kelly, J. Jagiello, T.J. Emge, J. Li, Achieving high density of adsorbed hydrogen in microporous metal organic frameworks, Adv. Mater. 17 (2005) 2703;
(b) A.C. Sudik, A.R. Millward, N.W. Ockwig, A.P. Côté, J. Kim, O.M. Yaghi, Design, synthesis, structure, and gas (N_2, Ar, CO_2, CH_4, and H_2) sorption properties of porous metal–organic tetrahedral and heterocuboidal polyhedra, J. Am. Chem. Soc. 127 (2005) 7110;
(c) A.G. Wong-Foy, A.J. Matzger, O.M. Yaghi, Exceptional H2 saturation uptake in microporous metal–organic frameworks, J. Am. Chem. Soc. 128 (2006) 3494;
(d) J.L.C. Rowsell, O.M. Yaghi, Effects of functionalization, catenation, and variation of the metal oxide and organic linking units on the low-pressure hydrogen adsorption properties of metal–organic frameworks, J. Am. Chem. Soc. 128 (2006) 1304;
(e) B. Panella, M. Hirscher, H. Pütter, U. Müller, Hydrogen adsorption in metal–organic frameworks: Cu–MOFs and Zn–MOFs compared, Adv. Funct. Mater. 16 (2006) 520.